

Non-hypertrophic chondrogenesis of mesenchymal stem cells through mechano-hypoxia programming

Journal of Tissue Engineering
Volume 14: 1–18
© The Author(s) 2023
Article reuse guidelines:
sagepub.com/journals-permissions
DOI: 10.1177/20417314231172574
journals.sagepub.com/home/tej



David Xinzheyang Li^{1,2*} , Zhiyao Ma^{1*},
Alexander RA Szojka¹ , Xiaoyi Lan^{1,2}, Melanie Kunze¹,
Ailette Mulet-Sierra¹, Lindsey Westover³ and
Adetola B Adesida¹ 

Abstract

Cartilage tissue engineering aims to generate functional replacements to treat cartilage defects from damage and osteoarthritis. Human bone marrow-derived mesenchymal stem cells (hBM-MSCs) are a promising cell source for making cartilage, but current differentiation protocols require the supplementation of growth factors like TGF- β 1 or - β 3. This can lead to undesirable hypertrophic differentiation of hBM-MSCs that progress to bone. We have found previously that exposing engineered human meniscus tissues to physiologically relevant conditions of the knee (mechanical loading and hypoxia; hence, mechano-hypoxia conditioning) increased the gene expression of hyaline cartilage markers, *SOX9* and *COL2A1*, inhibited hypertrophic marker *COL10A1*, and promoted bulk mechanical property development. Adding further to this protocol, we hypothesize that combined mechano-hypoxia conditioning with TGF- β 3 growth factor withdrawal will promote stable, non-hypertrophic chondrogenesis of hBM-MSCs embedded in an HA-hydrogel. We found that the combined treatment upregulated many cartilage matrix- and development-related markers while suppressing many hypertrophic- and bone development-related markers. Tissue level assessments with biochemical assays, immunofluorescence, and histochemical staining confirmed the gene expression data. Further, mechanical property development in the dynamic compression treatment shows promise toward generating functional engineered cartilage through more optimized and longer culture conditions. In summary, this study introduced a novel protocol to differentiate hBM-MSCs into stable, cartilage-forming cells.

Keywords

Engineered human cartilage, mechanical stimulation, dynamic compression, cyclic hydrostatic pressure, TGF-beta growth factor withdrawal, transcriptome

Date received: 28 November 2022; accepted: 9 April 2023

¹Department of Surgery, Faculty of Medicine and Dentistry, University of Alberta, Edmonton, AB, Canada

²Department of Civil and Environmental Engineering, Faculty of Engineering, AB, University of Alberta, Edmonton, AB, Canada

³Department of Mechanical Engineering, Faculty of Engineering, University of Alberta, Edmonton, AB, Canada

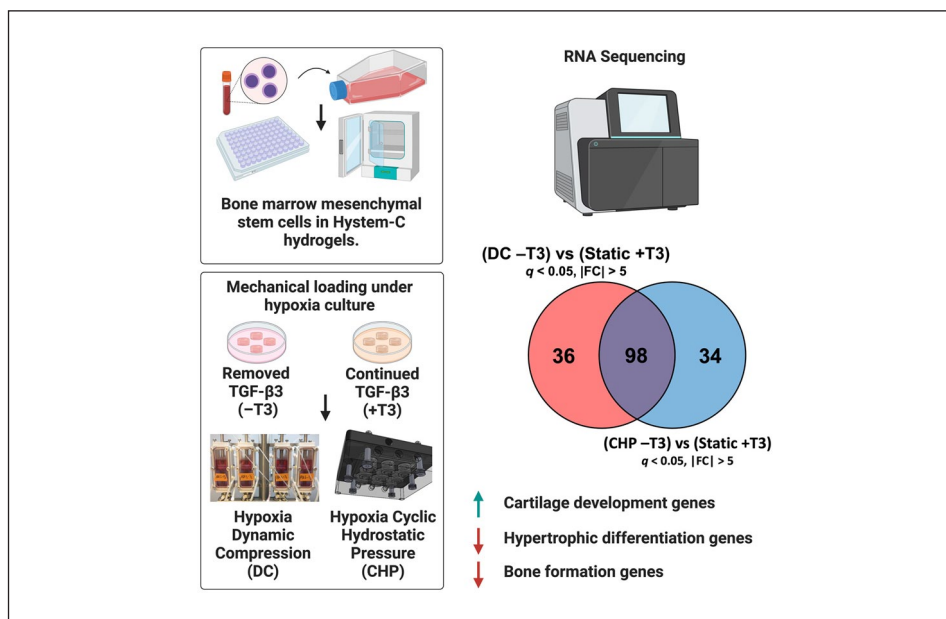
*These authors have contributed equally to this work and share first authorship.

Corresponding author:

Adetola B. Adesida, University of Alberta Faculty of Medicine and Dentistry, Li Ka Shing Centre for Health Research Innovation, Room 3.002E, Edmonton AB T6G 2E1, Canada.
Email: adesida@ualberta.ca



Graphical abstract



Introduction

Knee osteoarthritis (KOA) is the most common osteoarthritis afflicting >10% of the population and is one of the leading causes of physical disability.¹ Damaged articular cartilage (AC) of the knee is a risk factor for developing KOA.² AC is avascular and has a limited capacity for self-repair. Cell-based therapies using cell culture-expanded autologous AC forming cells (i.e. articular chondrocytes) from non-weight bearing (NWB) AC have shown promising clinical results post-implantation at focal defects.³⁻⁵ However, the extracellular matrix (ECM) produced by the implanted chondrocytes is inferior and does not recapitulate the mechanically competent ECM of native AC due to chondrocyte de-differentiation during cell expansion.^{6,7}

Mesenchymal stem cells (MSC) possess self-renewal and multilineage properties, including the ability to form chondrocytes and synthesize AC ECM after chondrogenesis.⁸⁻¹⁰ In addition, MSC are accessible at several less invasive anatomical sites compared to NWB AC, including bone marrow and adipose tissues. As such, MSC have attracted clinical interest for AC repair. However, the current protocols for the chondrogenic differentiation of MSC involve the addition of transforming growth factors (i.e. TGF- β 1 or - β 3)¹¹ and produce unstable hypertrophic chondrocytes that progress to bone in vivo through endochondral ossification.^{12,13} Although these growth factors have been shown in a plethora of studies to be necessary for the initial induction of chondrogenesis for various cell types,¹⁴⁻²¹ their presence may not be necessary throughout the entire culture duration. Bahcecioglu et al. have demonstrated that initial supplementation of TGF- β 1 following by its withdrawal led to increased production of collagen

by porcine fibrochondrocytes in a 3D-printed PCL/hydrogel construct under dynamic loading.¹⁶ Hennig et al. have also shown that increased concentrations of TGF- β 3 did not improve chondrogenesis of adipose-derived mesenchymal stem cells.²² Thus, growth factor withdrawal after initial supplementation may promote stable differentiation of MSC into chondrocytes while minimizing growth factor-induced chondrocyte hypertrophy.

It has long been known that the ECM of AC is central to its biomechanical function in the joint and the phenotype of the articular chondrocytes within.²³ Hyaluronan (HA) is a major component of AC's ECM.^{23,24} The cell surface antigen, CD44, is the main receptor of HA, and the interaction between HA and CD44 on articular chondrocytes is crucial for the homeostasis of AC.²³ It has been shown that HA-enriched microenvironment augmented the chondrogenesis of adipose-derived MSC through HA-CD44 interaction in the presence of TGF- β 1.^{25,26} The HA-CD44 interaction also mitigated the gene expression of type X collagen (*COL10A1*) – a marker of hypertrophic chondrocytes. Furthermore, our team has shown that hypoxic culture conditions (a physiologically relevant condition of the knee) of 3% O₂ enhanced the in vitro chondrogenesis of adipose and bone marrow-derived MSC (i.e. BM-MSC) in the presence of TGF- β 3^{27,28} and reduced the expression of *COL10A1* in BM-MSC.²⁸ Our preliminary data also showed that human BM-MSC (hBM-MSC) expressed CD44 regardless of whether the culture was at 3% or 21% O₂.²⁸

Mechanical stimulation plays a critical role in maintaining healthy cartilage.²⁹ Dynamic compression (DC) is one of the most widely used loading modalities in cartilage engineering due to its physiological relevance.^{14,16,30-34} Recent data from our lab suggests that exposing human

Table 1. Comparison breakdown for ANOVA of RNA sequencing data and the number of genes that meet each filter. Sequencing was performed on $n=3$ donors (M23, M42, and M58). Filters are applied additively from left to right.

Comparison		Number of genes after additively applying each filter			
		Total counts >150	$q < 0.05$	$ \text{FC} > 2$	$ \text{FC} > 5$
Experiment I: Static culture under different oxygen tensions	[HYP] vs [NRX]	8812	4707	894	106
	[-T3] vs [+T3]		1728	433	85
	[HYP -T3] vs [NRX +T3]		3878	1472	254
Experiment II: Mechanical loading under hypoxia culture	[DC] vs [Static]	9790	4822	684	53
	[CHP] vs [Static]		4071	117	39
	[DC -T3] vs [Static +T3]		2657	883	134
	[CHP -T3] vs [Static +T3]		2263	314	132

HYP: hypoxia (3% O₂); NRX: normoxia (20% O₂); -T3: TGF- β 3 withdrawal; +T3: TGF- β 3 continual; DC: dynamic compression; CHP: cyclic hydrostatic pressure; Static: static controls not loaded; q -values: adjusted p -values for the false discovery rate (FDR); |FC|: absolute fold change.

meniscal chondrocytes embedded in a collagen scaffold to mechanical loading using DC and hypoxia (hence, mechano-hypoxia conditioning) induced a strong pro-chondrogenic phenotype.³² The treatment strategy increased the mRNA expression of *SOX9*, an essential transcription factor for chondrogenesis,³⁵ and hyaline cartilage marker *COL2A1*, as well as inhibited hypertrophic marker *COL10A1*, and promoted bulk mechanical property development.³² Similarly, DC of mouse embryonic limb bud MSC within a collagen hydrogel promoted chondrogenesis through the induction of *SOX9* as well as the mRNA expression of other chondrogenic genes, including *COL2A1* and *ACAN*.³⁶ Another modality of loading is cyclic hydrostatic pressure (CHP), which mimics physiological loading patterns.^{37,38} A plethora of studies have shown that CHP applied to engineered tissues has induced pro-chondrogenic effects in various cell types, including human MSC.^{39–46}

Taking these altogether, we hypothesize that the combination of mechanical loading with hypoxia culture and TGF- β 3 growth factor withdrawal will promote stable, non-hypertrophic chondrogenesis of hBM-MSC embedded in an HA-hydrogel. To this end, we first assessed static hypoxia culture with growth factor withdrawal against static normoxia (20% O₂) culture at the global transcriptome and tissue matrix level. We then assessed two modalities of mechanical loading (dynamic compression, DC and cyclic hydrostatic pressure, CHP) with growth factor withdrawal against static culture, all under hypoxia.

Results

RNA-sequencing dataset overview

Transcriptome analysis included the global gene expression profiles of $n=3$ donors (M23, M42, M58), each exposed to the experimental conditions from Experiments I and II. Hypoxia (HYP) static culture samples were used for the independent analysis of both experiments. After preprocessing as described in the methods, 13,898 genes

were preserved for downstream analysis. Table 1 shows the comparison breakdown and the number of genes that meet the conditions of each filter and Supplemental Table S1 summarizes quality control metrics. The authenticity of the RNA-sequencing data was also validated against select RT-qPCR genes (Supplemental Figure S1), and the degree of correlation was determined with an R^2 value of 0.817, showing a strong correlation between the two transcription measurement methods.

Experiment I: Hypoxia and TGF- β 3 withdrawal under static culture promoted a non-hypertrophic phenotype of hBM-MSC

We first assessed static hypoxia (HYP, 3% O₂) culture with growth factor withdrawal against static normoxia (NRX, 20% O₂) culture at the global transcriptome and tissue matrix level. Unbiased principal component analysis (PCA) of the RNA-sequencing data indicated a clear separation for the oxygen tension and TGF- β 3 variables across PC1 and PC2, respectively, while the donor variable did not show good separation (Figure 1(a)). The first three PCs together explained 71.3% of the variance in Experiment I. Further, the heatmap of significant differentially expressed genes (DEGs) for the [HYP -T3] vs [NRX +T3] comparison similarly shows a strong separation in the clustering of samples for the oxygen tension and TGF- β 3 variables (Figure 1(b)). However, one sample (donor M58, HYP+T3) seemed to separate/cluster differently compared to the other samples in the group. Nonetheless, both experimental variables modulated a large number of DEGs, as indicated in Table 1. Moreover, the Venn diagram (Figure 1(c)) showed that hypoxia and TGF- β 3 withdrawal each modulated a unique panel of genes based on the small proportion that overlaps. The combined treatment of HYP -T3 modulated another unique set of DEGs while retaining the majority of DEGs from the individual treatments. This is supported by the volcano plots (Figure 1(d)–(f)), which show different labeled genes that are most

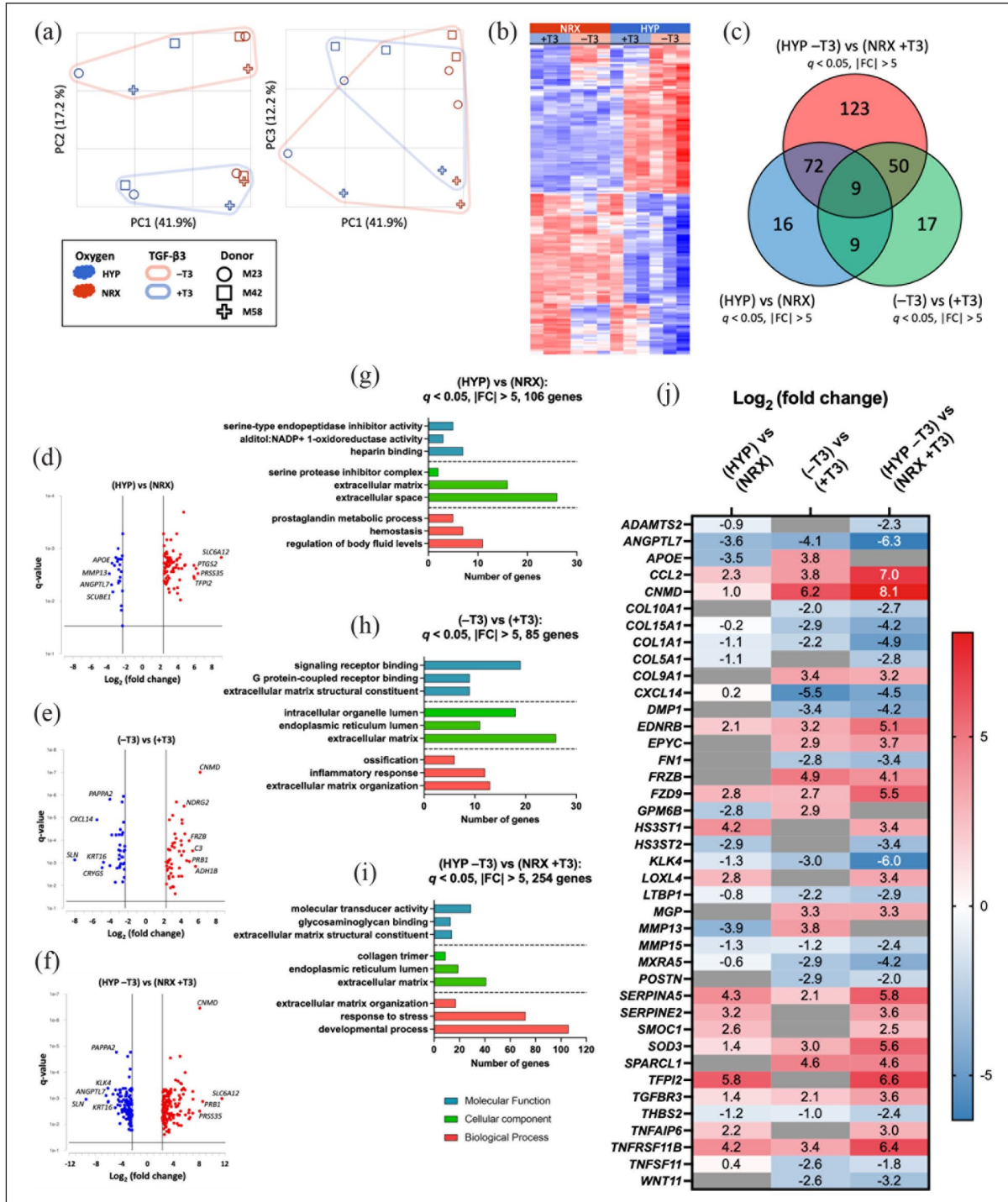


Figure 1. Experiment I: RNA-seq results suggest that hypoxia (3% O₂) and TGF- β 3 withdrawal under static culture promoted a non-hypertrophic phenotype of hBM-MSC. (a) Unbiased principal component analysis (PCA) plotting PC1-PC2 and PC1-PC3 for oxygen tension, TGF- β 3, and donor variables. (b) Heatmap of significant differentially expressed genes (DEGs) for the [HYP -T3] vs [NRX +T3] comparison with total counts > 150 , $q < 0.05$, and $|FC| > 2$ (1472 genes total). Genes (rows) and samples (columns) are clustered using the Euclidean method. (c) Venn diagram showing the overlap of significant DEGs between different comparisons. The top 15 highest up and downregulated genes in the [HYP -T3] vs [NRX +T3] comparison (123 genes) are shown in Supplemental Figure S2. (d-f) Volcano plots showing significant DEGs in each respective comparison with total counts > 150 , $q < 0.05$ (horizontal line crossing y-axis), and $|FC| > 5$ (vertical lines crossing x-axis). Some highest up and downregulated genes are labeled. (g-i) Top non-redundant Gene Ontology (GO) terms enriched by significant DEGs in each respective comparison. (j) Select panel of cartilage-related markers. Genes are chosen from previous knowledge and relevant GO terms (i.e. extracellular matrix). DEGs were determined using ANOVA for oxygen tension, TGF- β 3, and donor (random) variables. All cells with values on the color spectrum are statistically significant ($q < 0.05$) and gray cells without values are non-significant.

up and downregulated in each comparison. Further, the top highest up and downregulated genes (Supplemental Figure S2) unique to each treatment (i.e. from the 16, 17, and 123 genes of the Venn diagram) show that the combined treatment appears to be the additive effect from the individual hypoxia and TGF- β 3 withdrawal effects. The top non-redundant Gene Ontology (GO) terms enriched by significant DEGs suggest that TGF- β 3 withdrawal modulated genes that function in “ossification” and “inflammatory response” among others. The combined treatment of HYP-T3 also promoted functions related to ECM development and organization (Figure 1(g)–(i)).

The combined treatments of hypoxia and TGF- β 3 withdrawal under static culture induced a strong anti-hypertrophic phenotype of hBM-MSC, as evident in the panel of select genes (Figure 1(j)) related to cartilage development. Namely, hypertrophy markers *COL10A1* (downregulated 6.5-fold) and *MMP13* (not significant) were suppressed or not regulated in the combined treatment. TGF- β 3 withdrawal also upregulated *FRZB*, an antagonist of Wnt signaling⁴⁷ and an inhibitor for hypertrophy, by 17-fold as well as upregulating *MGP*, an inhibitor to bone formation,⁴⁸ by 9.8-fold. Other factors that function toward osteoblast differentiation,^{49,50} such as *DMP1* (downregulated 18-fold), *FNI* (downregulated 11-fold), and *GPM6B* (not significant), were suppressed or not regulated in the combined treatment. Further, *THBS2*, a ligand for the CD36 receptor,⁵¹ which is implicated in the development of osteoarthritis,^{52,53} was downregulated 5.3-fold. The ratio of *TNFRSF11B* (or *OPG*) to *TNFSF11* (or *RANKL*), an inhibitor and promoter of osteoclast activation,⁵⁴ respectively, was also highly positive in the combined treatment suggesting a strong response away from osteoclast differentiation. Interestingly, the TGF- β 3 gene (*TGFB3*) was not significantly regulated, but the receptor gene *TGFB3R* was upregulated 12-fold in the combined treatment. Further, *TGFB1* and *TGFBRI* were both downregulated (2.35- and 1.51-fold, respectively), while *TFGB2* and *TGFBRI2* were both upregulated (5.16- and 1.62-fold, respectively) (data not shown). Finally, various markers related to ECM reorganization, such as *EPYC*, *MMP15*, *ADAMTS2*, *MXRA5*, *SPARCL1*, and *TNFAIP6*, were modulated to varying degrees.

The suppression of hypertrophy from combined hypoxia and TGF- β 3 withdrawal is confirmed by the RT-qPCR results, where a clear suppression of *COL10A1* is seen (Figure 2(d)). Further, hypoxia and TGF- β 3 withdrawal appear to upregulate chondrogenic markers *ACAN*, *COL2A1* (Figure 2(a) and (c)), and *COL2A1* to *COL1A2* ratio (Supplemental Figure S3 A, B). These findings are confirmed by the histological (Figure 2(h)) and biochemical analyses (Supplemental Figures S4 and S5 A, B), where staining for type II collagen and type X collagen appears to be upregulated and downregulated, respectively, while the measured GAG/DNA ratio is higher in the TGF- β 3 withdrawal groups. However, donor-to-donor

variability is high, and staining quantification results did not show any statistical significance between groups (Figure 2(i)–(k)). However, it appears that combined HYP-T3 showed increased collagen type II and reduced collagen type X for every donor (Supplemental Figure S5 C, D). Safranin-O staining (Figure 2(h)) for sulfated glycosaminoglycans (sGAG) also showed highly positive staining at baseline and post-experiment for all samples. It should be noted that the lightly stained safranin-O sections are likely due to the differential dehydration of the hydrogel tissues in the preprocessing procedure prior to staining and not from experimental variables. Finally, the combined treatments did not promote the development of mechanical properties, as both peak and equilibrium moduli are not significantly different across the groups (Supplemental Figure S4).

Experiment II: Mechanical stimulation and TGF- β 3 withdrawal under hypoxia promoted a strong chondrogenic and non-hypertrophic phenotype of hBM-MSC

After confirming that combined hypoxia and TGF- β 3 withdrawal induced a strong anti-hypertrophic phenotype of hBM-MSC, we assessed two modalities of mechanical loading (dynamic compression, DC and cyclic hydrostatic pressure, CHP) with TGF- β 3 withdrawal against static culture, all under hypoxia. Unbiased principal component analysis (PCA) of the RNA-sequencing data indicated a clear separation for the mechanical loading and TGF- β 3 variables across PC1 and PC2, respectively, while the donor variable did not show good separation (Figure 3(a)). DC and CHP were clustered together but highly separated from the static controls suggesting that the two modalities of loading induced similar effects. The first three PCs together explained 60.8% of the variance in Experiment II. Further, the heatmap of significant differentially expressed genes (DEGs) for the [DC-T3] vs [Static+T3] and [CHP-T3] vs [Static+T3] comparisons similarly show a strong separation in the clustering of samples for the mechanical loading and TGF- β 3 variables (Figure 3(b)). Here, DC and CHP also clustered together but away from the static controls. However, one sample (donor M58, Static+T3) seemed to separate/cluster differently compared to the other samples in the group. Nonetheless, both experimental variables modulated a large number of DEGs, as indicated in Table 1. The Venn diagram (Figure 3(c)) also showed that DC with TGF- β 3 withdrawal and CHP with TGF- β 3 withdrawal modulated a similar panel of genes based on the large proportion that overlaps. This is supported by the volcano plots (Figure 3(f) and (g)), which show similar labeled genes that are most up and downregulated in each treatment. Further, the top highest up and downregulated genes (Supplemental Figure S6) unique to each treatment (i.e. from the 36 and 34 genes of the Venn

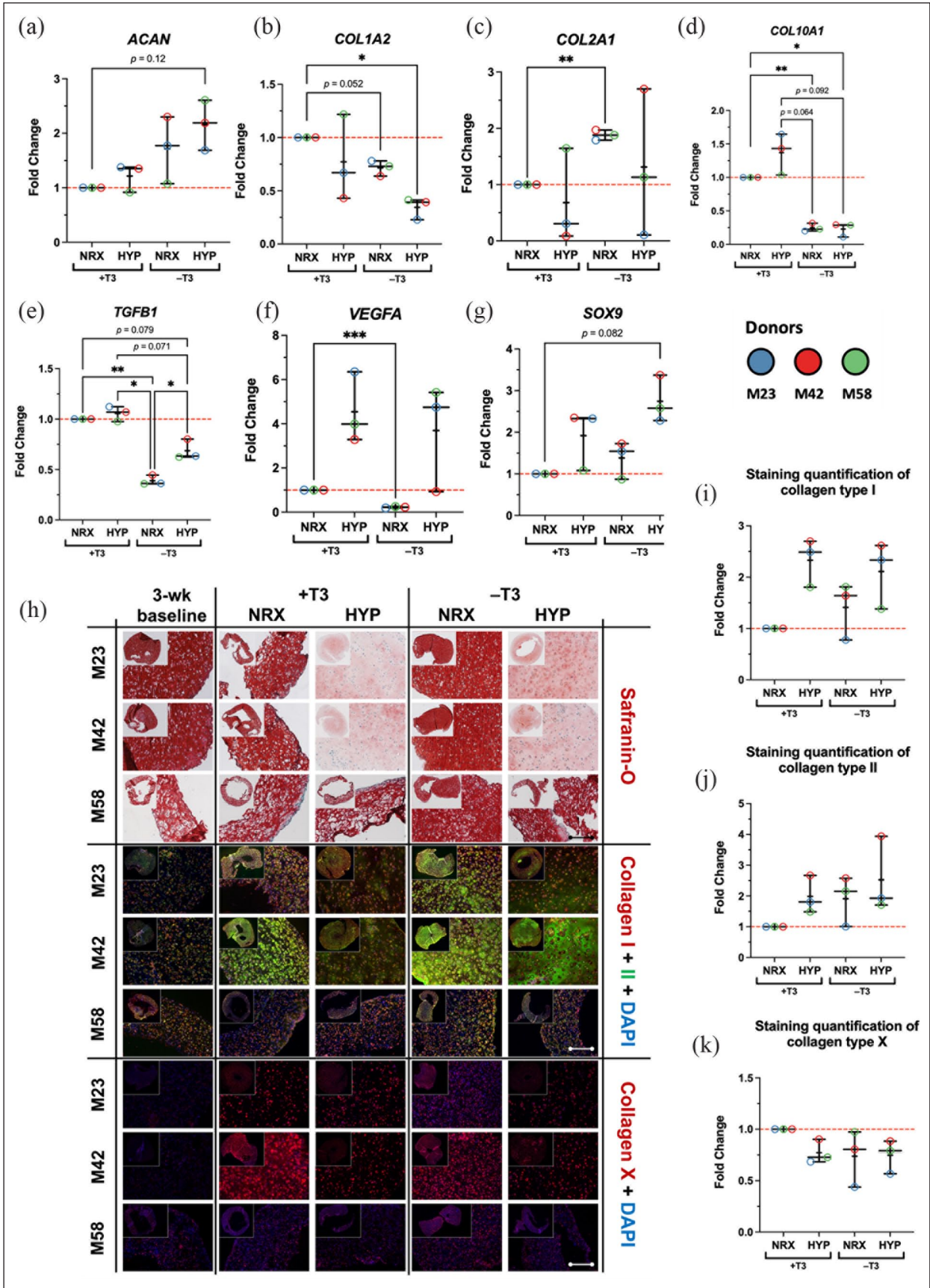


Figure 2. (Continued)

Figure 2. (Continued). Experiment I: tissue level and RT-qPCR confirms that hypoxia (3% O₂) and TGF-β3 withdrawal under static culture promoted a non-hypertrophic phenotype of hBM-MSC. (a–g) Regulation of selected gene markers as measured by RT-qPCR. Fold changes are reported as expression values normalized to the [NRX + T3] group. (h) Histological and immunofluorescence staining analysis. Differences in Safranin-O staining for M23 and M42 hypoxia samples may be a result of the differential dehydration of the hydrogels in tissue preprocessing prior to paraffin-embedding. Scale bar represents 300 μm. Corner images showing complete sections are not to scale. (i–k) Quantification of immunofluorescence images for Collagen Type I, Type II and Type X respectively. Fold changes are reported as quantified values normalized to the [NRX + T3] group and quantification was conducted with a Python script. Statistics was performed using a one-way ANOVA (with the Geisser-Greenhouse correction and Tukey's multiple comparison test). Significance levels are represented as * $p < 0.05$, ** $p < 0.01$, and *** $p < 0.001$. Groups are plotted as box and whisker plots showing min to max of all points and "+" represent the mean value.

diagram) showed that the majority of genes were regulated in the same direction and by similar magnitudes by DC and CHP treatments. Further, the top non-redundant Gene Ontology (GO) terms enriched by significant DEGs suggest that both loading modalities with TGF-β3 withdrawal modulated genes that function related to cartilage development and ECM organization (Figure 3(d) and (e)).

The combined treatments of mechanical loading (both DC and CHP) with TGF-β3 withdrawal induced a strong chondrogenic and non-hypertrophic phenotype of hBM-MSC as evident in the panel of select genes (Figure 3(h)) related to cartilage development. Namely, chondrogenic markers *ACAN*, *CNMD*, *COL2A1*, *COL9A1/2/3*, *COL11A1/2*, *COL14A1*, *HAPLN1*, *MATN3*, *MATN4*, and *SOX9* were all highly upregulated by mechanical loading with TGF-β3 withdrawal. Further, chondrocyte regulators *ASPN*, *CHADL*, *SNORC*,⁵⁵ and *TNC*,⁵⁶ which are involved in chondrocyte development and maturation, were also highly upregulated. Hypertrophic marker *COL10A1* was not significantly modulated, and *NOG*, an inhibitor to chondrocyte differentiation,^{57,58} was downregulated 7.5-fold from both mechanical loading combined treatments. Moreover, *FRZB*, an antagonist of Wnt signaling⁴⁷ and an inhibitor for hypertrophy, was highly upregulated (23-fold in DC-T3 and 49-fold in CHP-T3), while *LGR6*, a marker activated by Wnt signaling,⁵⁹ was highly downregulated (64-fold in DC-T3 and 104-fold in CHP-T3). *SMOC1*, an osteoblast regulator,⁶⁰ and *RARB*, a factor required for skeletal growth,⁶¹ were also both highly downregulated. Additionally, *MGP*, an inhibitor for bone formation,⁴⁸ was upregulated (4.6-fold in DC-T3 and 7.5-fold in CHP-T3), while *GDF10*, a factor that plays an inhibitory role in osteoblast differentiation,⁶² was the most upregulated gene (724-fold in DC-T3 and 446-fold in CHP-T3) from both mechanical loading combined treatments. Finally, various markers related to ECM reorganization, such as *EPYC*, *LAMA4*, *MMPI1*, *MMP7*, *NID2*, and *POSTN*, were modulated to varying degrees.

The induction of a chondrogenic and non-hypertrophic phenotype from combined mechanical loading and TGF-β3 withdrawal is confirmed by the RT-qPCR results (Figure 4(a)–(h)). Expression levels of *ACAN*, *COL2A1*, *SOX9*, and *COL2A1* to *COL1A2* ratio (Supplemental Figure S3 C, D) were all higher, while *COL10A1* levels

were lower in the TGF-β3 withdrawal groups. These findings are confirmed by the histological (Figure 4(i)) and biochemical analyses (Figure 4(a)–(d)), where staining for type II collagen and type X collagen appears to be upregulated and downregulated, respectively, while the measured GAG/DNA ratio is higher in the TGF-β3 withdrawal groups. Once again, donor-to-donor variability is high, and staining quantification results did not show any statistical significance between groups (Figure 4(j)–(l)). However, it appears that combined DC-T3 or CHP-T3 showed increased collagen type II and reduced collagen type X for most of the donors (Supplemental Figure S5 G, H). Safranin-O staining (Figure 4(i)) for sGAG also showed highly positive staining at baseline and post-experiment for all samples. It should be noted that the lightly stained safranin-O sections are likely due to the differential dehydration of the hydrogel tissues in the preprocessing procedure prior to staining and not from experimental variables. Finally, DC treatments produced tissues with significantly higher peak (Figure 5(e), Supplemental Figure S5 I) and equilibrium moduli (Figure 5(f)), while CHP resulted in marginally higher values. However, the magnitude of these values is still lacking when compared to native articular cartilage mechanical properties.

Combined mechanical loading (DC or CHP) with TGF-β3 withdrawal regulated genes that were present in key KEGG pathways. In particular, TGF-Beta Signaling Pathway (Figure 6(b) and (c)), Focal Adhesion (Figure 6(d) and (e)), and PI3K-AKT Signaling Pathway (Figure 6(f) and (g)) were among the most enriched pathways (Figure 6(a)). In the TGF-Beta Signaling Pathway, many Smad factors were regulated along with the cell-receptor inhibitor *BAMBI*. In Focal Adhesion, many ECM factors and growth factor genes were regulated as well as factors contributing to ECM organization. In the PI3K-AKT Signaling Pathway, many cell surface receptors such as GPCRs, ITGAs, CytokineR, TLRs, and RTKs were significantly regulated.

Discussion

This study introduced a novel protocol to differentiate human bone marrow-derived mesenchymal stem cells (hBM-MSC) into stable, cartilage-forming cells. We

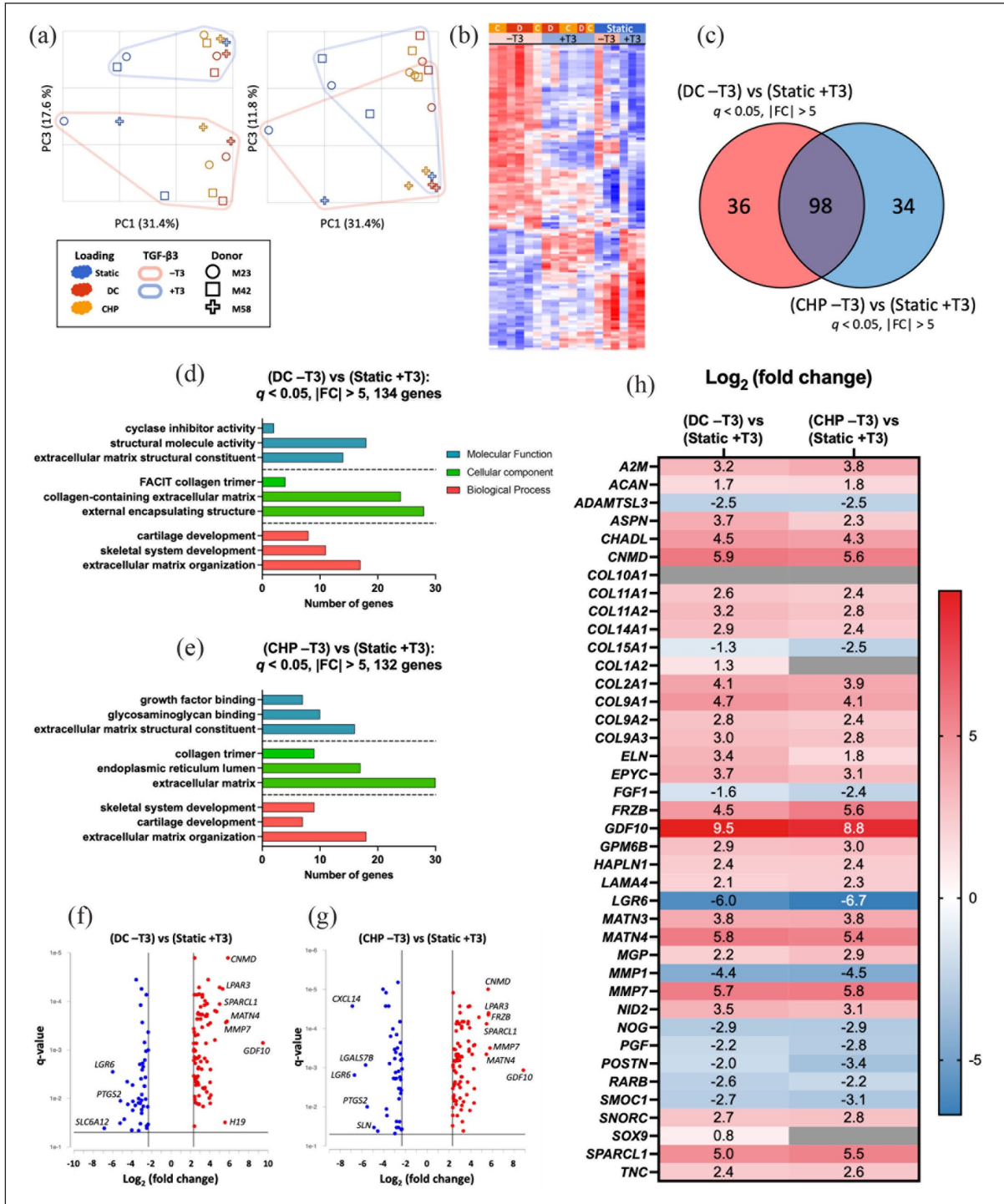


Figure 3. Experiment II: RNA-seq results suggest that mechanical stimulation and TGF- β 3 withdrawal under hypoxic (3% O_2) culture promoted a strong chondrogenic and non-hypertrophic phenotype of hBM-MSC. (a) Unbiased principal component analysis (PCA) plotting PC1-PC2 and PC1-PC3 for mechanical loading, TGF- β 3, and donor variables. (b) Heatmap of significant differentially expressed genes (DEGs) for the [DC -T3] vs [Static +T3] and [CHP -T3] vs [Static +T3] comparison with total counts > 150 , $q < 0.05$, and $|FC| > 2$ (1071 genes total). Genes (rows) and samples (columns) are clustered using the Euclidean method. (c) Venn diagram showing the overlap of significant DEGs between different comparisons. The unique genes in the [DC -T3] vs [Static +T3] comparison (36 genes) and the [CHP -T3] vs [Static +T3] comparison (34 genes) are shown in Supplemental Figure S6. (d and e) Top non-redundant Gene Ontology (GO) terms enriched by significant DEGs in each respective comparison. (f and g) Volcano plots showing significant DEGs in each respective comparison with total counts > 150 , $q < 0.05$ (horizontal line crossing y-axis), and $|FC| > 5$ (vertical lines crossing x-axis). Some highest up and downregulated genes are labeled. (h) Select panel of cartilage-related markers. Genes are chosen from previous knowledge and relevant GO terms (i.e. extracellular matrix). DEGs were determined using ANOVA for mechanical stimulation, TGF- β 3, and donor (random) variables. All cells with values on the color spectrum are statistically significant ($q < 0.05$) and gray cells without values are non-significant.

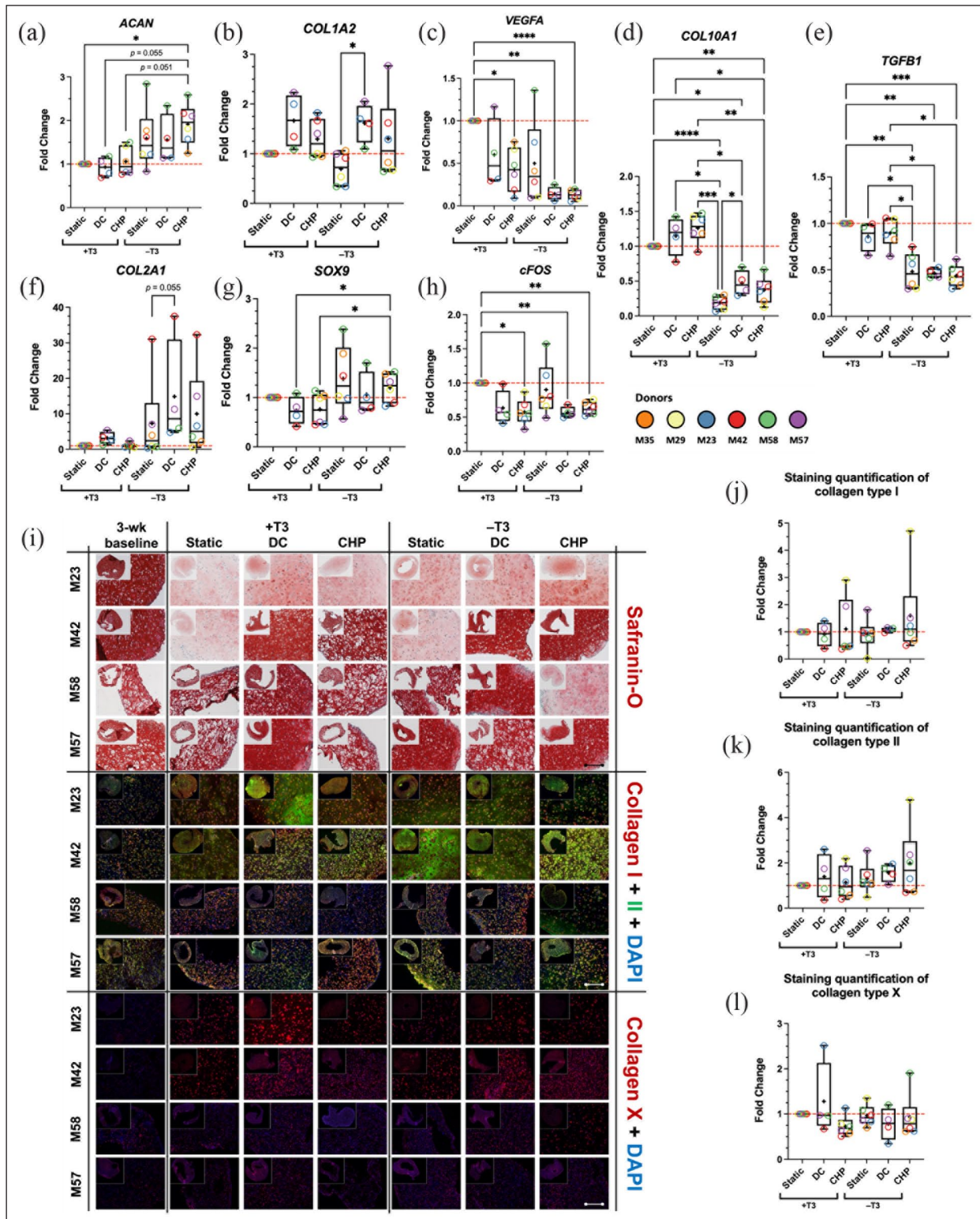


Figure 4. Experiment II: tissue level and RT-qPCR confirms that mechanical stimulation and TGF- β 3 withdrawal under hypoxic (3% O_2) culture promoted a strong chondrogenic and non-hypertrophic phenotype of hBM-MSC. (a–h) Regulation of selected gene markers as measured by RT-qPCR. Fold changes are reported as expression values normalized to the [Static +T3] group. (i) Histological and immunofluorescence staining analysis. Differences in Safranin-O staining for M23, M42, and M58 samples may be a result of the differential dehydration of the hydrogels in tissue preprocessing prior to paraffin-embedding. Images for the 3-week baseline, Static -T3, and Static +T3 groups for donors M23, M42, and M58 are identical to the 3-week baseline, HYP

Figure 4. (Continued)

Figure 4. (Continued)

–T3, and HYP + T3 group images used in Figure 4(h) as those same samples were used for analysis in both experiments. Scale bar represents 300 μm . Corner images showing complete sections are not to scale. (j–l) Quantification of immunofluorescence images for Collagen Type I, Type II and Type X respectively. Fold changes are reported as quantified values normalized to the [Static + T3] group and quantification was conducted with a Python script. Statistics was performed using a one-way ANOVA (with the Geisser-Greenhouse correction and Tukey's multiple comparison test). Significance levels are represented as $*p < 0.05$, $**p < 0.01$, $***p < 0.001$, and $****p < 0.0001$. Groups are plotted as box and whisker plots showing min to max of all points and “+” represent the mean value.

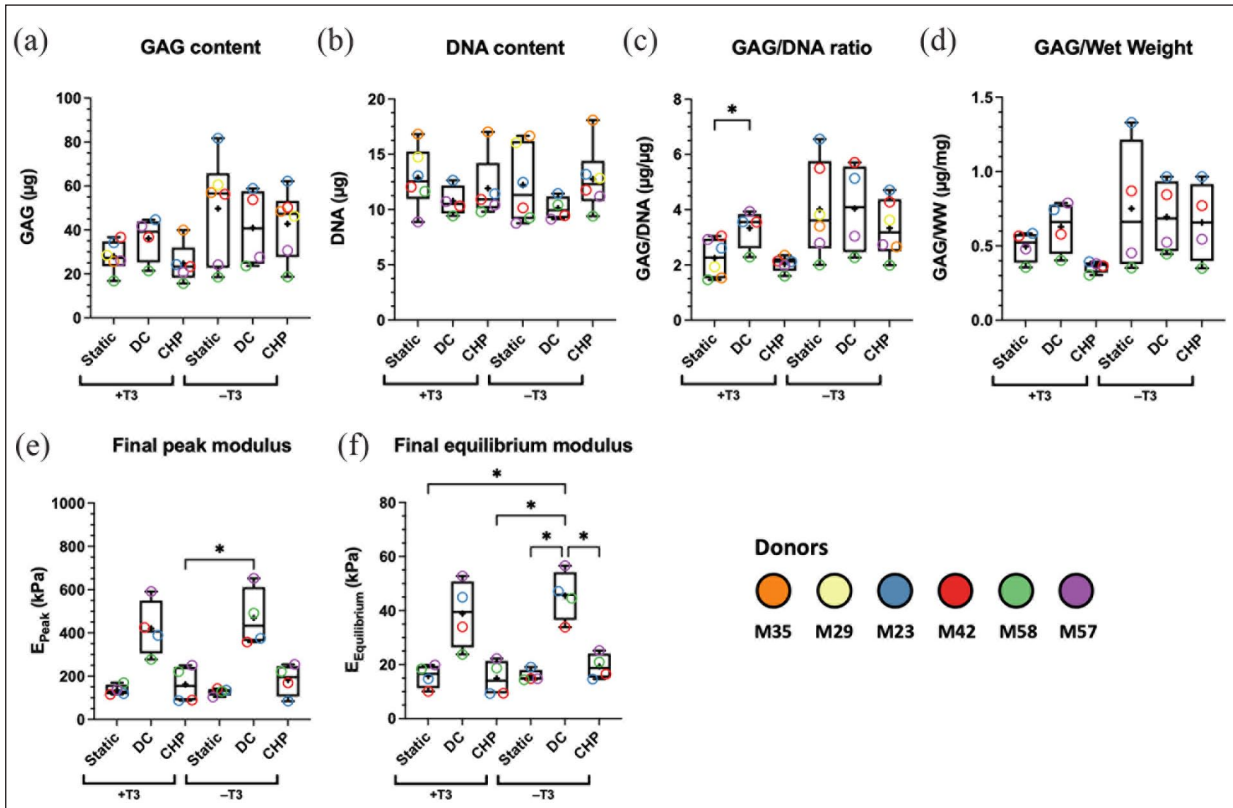


Figure 5. Experiment II: samples showed increased mechanical properties after dynamic compression (DC) loading. (a) Measured glycosaminoglycan (GAG) content. (b) Measured DNA content. (c) Measured GAG to DNA ratio. (d) Measured GAG to wet weight ratio. (e) Measured final peak modulus. (f) Measured final equilibrium modulus. Statistics was performed using a one-way ANOVA (with the Geisser-Greenhouse correction and Tukey's multiple comparison test). Significance levels are represented as $*p < 0.05$ and $**p < 0.01$. Groups are plotted as box and whisker plots showing min to max of all points, and “+” represent the mean value.

hypothesized that the combination of mechanical loading from dynamic compression (DC) and cyclic hydrostatic pressure (CHP) with hypoxia culture and TGF- β 3 growth factor withdrawal would promote non-hypertrophic chondrogenesis of hBM-MSC embedded in an HA-hydrogel. As an attractive cell source for regenerative medicine, hBM-MSC are characterized by their accessibility, expansion capacity, and high pluripotency. Considerable efforts have been directed at inducing the stable chondrogenic differentiation of hBM-MSC. Given the complex nature of cartilage tissue formation, this process requires stimulation from both biochemical and biomechanical cues. In addition, the spatial and temporal profiles of applied cues also play a critical role in the outcome of engineered

tissues. Global transcriptome and tissue level assessments from this study showed that the withdrawal of TGF- β 3 after initial supplementation, in combination with mechanical loading and hypoxia, induced a cartilage-like phenotype in hBM-MSC seeded tissue constructs while suppressing hypertrophic differentiation.

Transforming growth factor-beta (TGF- β) is a polypeptide growth factor superfamily composed of three isoforms (TGF- β 1, - β 2, and - β 3).⁶³ TGF- β is essential in nearly every aspect of cartilage formation and development, and it is the most used growth factor in chondrogenic medium.^{64–67} Among the three isoforms, TGF- β 3 is well demonstrated as a necessary mediator for the chondrogenic differentiation of MSC and promotes the

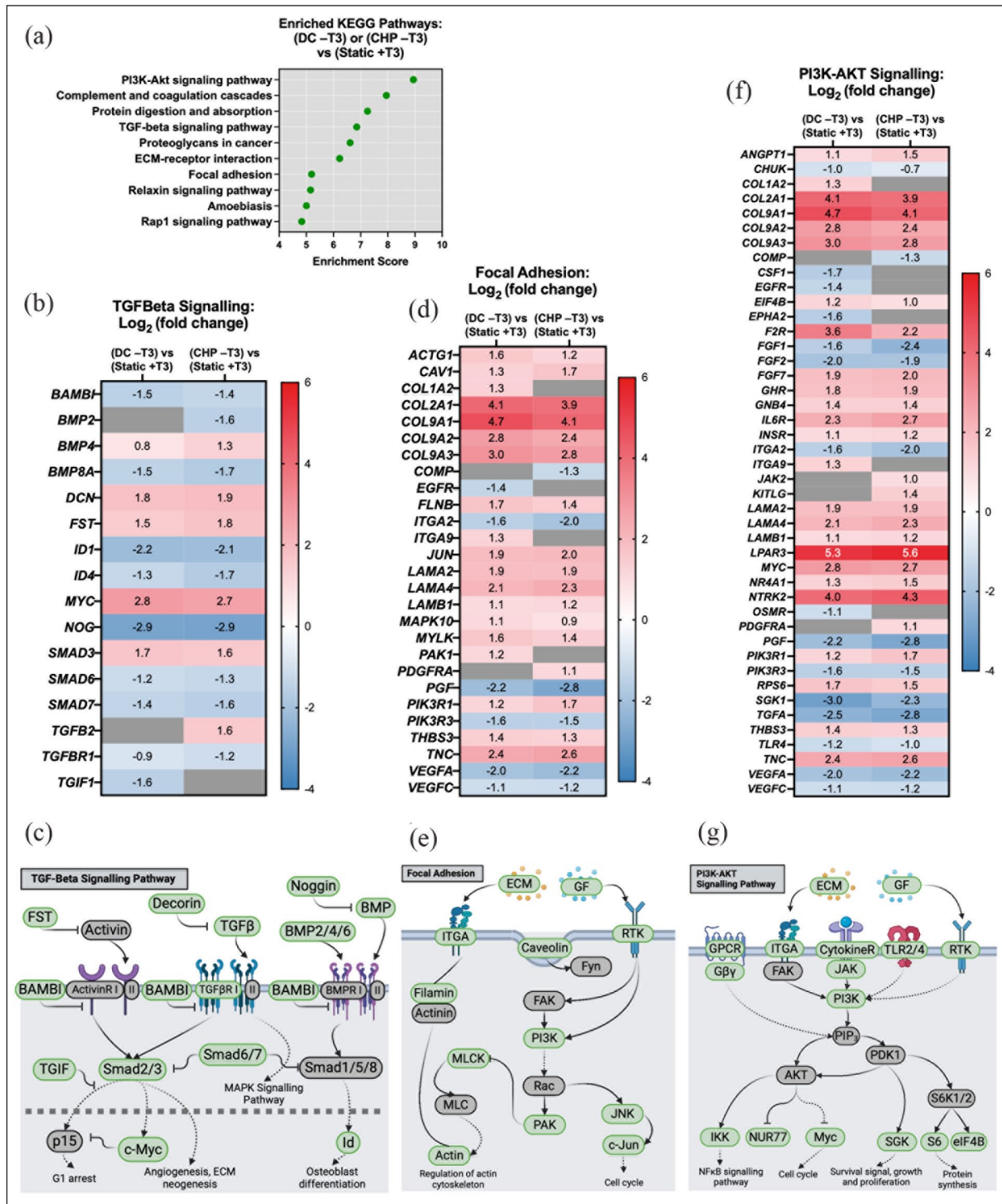


Figure 6. Experiment II: RNA-sequencing results show key pathways that are modulated by mechanical stimulation and TGF-β3 withdrawal under hypoxic (3% O₂) culture. (a) Top KEGG pathways enriched by differentially expressed genes (DEGs) for the [DC -T3] vs [Static +T3] and [CHP -T3] vs [Static +T3] comparison. (b) Significant DEGs modulated in the TGF-Beta Signaling Pathway. (c) Simplified schematic of key genes/factors that are modulated in the TGF-Beta Signaling Pathway. (d) Significant DEGs modulated in the Focal Adhesion pathway. (e) Simplified schematic of key genes/factors that are modulated in the Focal Adhesion pathway. (f) Significant DEGs modulated in the PI3K-AKT Signaling Pathway. (g) Simplified schematic of key genes/factors that are modulated in the PI3K-AKT Signaling Pathway. DEGs were determined using ANOVA for mechanical stimulation, TGF-β3, and donor (random) variables. All cells with values on the color spectrum are statistically significant ($q < 0.05$) and gray cells without values are non-significant. Green icons in simplified pathway schematics are statistically significant and gray icons are not significant. Solid arrows represent direct relationship and dashed arrows indicate there are additional factors not shown.

deposition of cartilage-like ECM components such as GAG and collagens.^{14,68,69} Even though the molecular mechanism of TGF- β 3 in chondrogenesis is not fully understood, it is proposed that the chondrogenesis driving effect of TGF- β 3 is due to the involvement of master chondrogenic transcription factor *SOX9*.⁷⁰ Upon the activation of the TGF- β receptor, intracellular molecules from the Smad family (Smad 2, Smad 3, and Smad 4) are phosphorylated and migrate to the nucleus as a heteromeric complex. The expression of target genes is then regulated by the complex through the Smad-binding elements.⁷⁰ The involvement of Smad molecules in the TGF- β 3 signaling pathway is confirmed in this study as several Smad molecules were significantly regulated by the combined treatment of mechanical loading with TGF- β 3 withdrawal (Figure 6(b)). Moreover, the expression level of *SOX9* also showed a significant difference between the withdrawal and continuous TGF- β 3 supplemented groups (Figures 3(h) and 4(g)).

It has been demonstrated that without the supplementation of TGF- β 3, the chondrogenesis of MSC seeding on a type I collagen could not be initiated, and cartilaginous ECM components failed to accumulate.¹⁴ However, chondrogenesis induced in MSC by TGF- β 3 is also accompanied by an early onset of hypertrophic differentiation, which is undesired for cartilage tissue engineering.^{13,71} Several factors may explain why TGF- β 3 withdrawal in this study induced the stable, non-hypertrophic chondrogenesis of hBM-MSC. Firstly, the development of cartilage tissue in vivo has been shown to be based on the time-dependent formation of several different components. The formation of collagen fibers is observed first during pre- and neonatal developmental stages, while GAG deposition occurs at a later phase.^{72,73} This sequential formation of cartilage components has been validated in an in vitro MSC pellet model using TGF- β ,⁷⁴ where the rapid accumulation of GAG occurs after the production of other chondrogenic markers.⁷⁴ TGF- β is proposed to regulate the synthesis of GAG⁷⁴ and proliferation of MSC in a concentration-dependent manner,⁷⁵ and the early or excessive deposition of GAG is believed to have an inhibitive effect on the formation of collagen fibers.⁷⁶ Thus, the optimal level of TGF- β for chondrogenesis is proposed to be a relatively low level to allow the development of collagen fibers and follow the temporal profile of normal cartilage development.⁷⁵ In our study, TGF- β 3 withdrawal may have kept the growth factor concentration at an optimally low level after initial matrix deposition during pre-culture to allow for the formation of cartilage components in sequential order. However, time-course measurements of these markers at the transcriptome and protein level are needed to confirm this. Another possible mechanism is the positive-feedback activation of the endogenously produced latent TGF- β with TGF- β 3 acting as an initiator.⁷⁷

This allows for the accumulation of growth factors over time, and the deposition of GAG can gradually take a dominant role over collagen formation. On the other hand, with the continuous supplementation of TGF- β 3, the gradual increase of growth factors over time is replaced by a constant high level, which may lead to an early deposition of GAG that prevents the formation of standard collagen fibers. In addition to biochemical cues, biomechanical cues are also critical for optimizing cartilage tissue engineering. Although the activation mechanism of latent TGF- β is still not clear, it is proposed that through the upregulation of proteolytic moieties such as plasmin and stromelysin-1 production, mechanical stimulation might further stimulate the activation of latent TGF- β .⁷⁸

There were several limitations in this study. Firstly, other morphological features that may be characteristic of hypertrophic chondrocytes, such as increased cell size or changes in cell shape, were not considered. However, we feel that our whole-tissue assessment is sufficient, particularly from the presence/absence of collagen type X, which is a more definitive approach for assessing hypertrophic chondrocytes. Further, trends from the immunofluorescence data were not supported statistically by the semi-quantification of the staining, and we attribute this mainly to the limitation of the staining quantification methodology. The staining quantification was only meant as supplemental to the histological data, and the results from the staining quantification depended on the particular tissue sections used. We also observed differential dehydration of the hydrogel constructs in tissue preprocessing prior to paraffin embedding such that some constructs contracted more than others. However, the GAG content and GAG/DNA ratio for these donors (M23 and M42) do not show significant decreases as compared to the other donors within the same treatment group. Finally, due to the high donor-to-donor variability within our donor cohort, many assessments failed to yield statistically significant results despite every or almost every donor showing a similar trend in the combined treatment groups as compared to controls. As we used a paired one-way ANOVA for the majority of our assessments, the high donor-to-donor variability will substantially reduce the statistical power. Overall, definitive conclusions were not based on the histological data alone, but rather, they are based on an overall assessment of all the data, including gene expression, histological, and biochemical analyses.

In summary, our data suggest that our proposed protocol using hypoxia, mechanical loading, and TGF- β 3 withdrawal allows for the stable differentiation of hBM-MSC to chondrocytes through the upregulation of many cartilage-related markers while suppressing hypertrophic markers. Future experiments will include in vivo implantation of engineered cartilage using this protocol to evaluate in vivo phenotype stability.

Experimental section/methods

The experimental overview is described in Supplemental Figure S7. Most culture methods and assays were performed identically to previously published studies.^{28,32,33,79–81}

Ethics statement and tissue procurement

Experimental methods and tissue procurement were conducted with approval from the University of Alberta's Health Research Ethics Board-Biomedical Panel (Study ID: Pro00018778). Human bone marrow-derived mesenchymal stem cells (hBM-MSC) were isolated from bone marrow aspirates obtained from non-osteoarthritic male patients ($n=6$ donors, 23–58 years old) undergoing routine orthopedic procedures. Donor details are summarized in Supplemental Table S2.

Cell and tissue pre-culture in hyaluronan-based hydrogel

Cell isolation and expansion were performed as described in previously published studies.^{28,79} Briefly, hBM-MSC were expanded in alpha minimum essential medium (α -MEM) supplemented with 10% v/v heat-inactivated fetal bovine serum (FBS), 100 mM 4-(2-hydroxyethyl)-1-piperazineethanesulfonic acid (HEPES), 1 mM sodium pyruvate (Sigma-Aldrich Co., MO, USA), 100 U/mL penicillin, 100 μ g/mL streptomycin, 0.29 mg/mL glutamine (PSG; Life Technologies, ON, Canada), and 5 ng/mL of fibroblast growth factor (FGF-2; Neuromics, MN, USA, #PR80001) under hypoxic (HYP) humidified conditions (3% O₂, 5% CO₂). They were stored in liquid nitrogen after passage 1 and then further expanded to passage 2 under HYP.

HyStem[®]-C (Advanced BioMatrix, CA, USA, #GS1005) is a cell-compatible, hyaluronan-based hydrogel crosslinked using thiol-reactive poly(ethylene glycol) diacrylate (PEGDA) and thiol-modified denatured porcine collagen. Hydrogels were prepared according to the manufacturer's protocols, and no measurable glycosaminoglycan (GAG) or DNA contents were seen in the hydrogels (data not shown). Expanded hBM-MSC were mixed into the hydrogel and cast into standard 96-well flat-bottom low attachment plates at a density of 5×10^6 cells/cm³ to form cylindrical tissue constructs (diameter=6 mm, height=2.5 mm). Cell-seeded hydrogels were pre-cultured in an X3 incubator system (Biospherix, USA) for 3 weeks under HYP for baseline matrix formation using a defined serum-free chondrogenic growth medium (HG-DMEM supplemented with HEPES, PSG, ITS +1 premix (Corning, Discovery Labware, Inc, MA, USA), 125 μ g/mL human serum albumin, 100 nM dexamethasone, 365 μ g/mL ascorbic acid 2-phosphate, 40 μ g/mL L-proline) and supplemented with 10 ng/mL of TGF- β 3 growth factor (Proteintech Group, USA, #HZ-1090). A trial group

(1 technical replicate) had TGF- β 3 removal during this 3-week pre-culture. However, preliminary live/dead assay results suggest that cells require the growth factor during pre-culture to preserve viability (Supplemental Figure S8). Thus, all tissues had TGF- β 3 supplemented during pre-culture.

Live/dead assay

After 3 weeks of pre-culture, the cell viability of hBM-MSC with and without the supplement of TGF- β 3 in Hystem-C hydrogel was assessed by Syto 13/Propidium iodide (PI) staining. Syto 13 (S7575, Thermo Fisher Scientific, Canada) stains the live-cell in green fluorescent, and PI (P3566, Thermo Fisher Scientific, Canada) stains the dead-cell in red fluorescent. Each construct was incubated in 1 mL PBS solution with 6.25 μ M Syto 13 and 15 μ M PI at room temperature for 30 min. The cell viability was visualized using Nikon confocal laser scanning microscope (Leica TCS SP5). Fluorescence was quantified using a Python script.

Experiment I variables: Oxygen tension and TGF- β 3 withdrawal

Baseline tissues (from $n=3$ donors) were randomly assigned to the TGF- β 3 withdrawal ($-T3$), or the TGF- β 3 continued ($+T3$) group, where the growth factor was either removed or supplemented in the chondrogenic growth medium, respectively. Tissues in each group were further randomly assigned to the hypoxia (HYP, 3% O₂) or normoxia (NRX, 20% O₂) group resulting in four experimental groups: HYP $-T3$, HYP $+T3$, NRX $-T3$, NRX $+T3$. Tissues under each experimental group condition were cultured statically in non-attachment Petri-dishes with approximately 7.5 mL of medium per tissue construct (to equate the required volume of media for Experiment II bioreactors), and media was changed once per week. Tissues were cultured for 3 weeks before harvest, and gene expression samples (2–3 technical replicates) were stored in TRIzol reagent (ThermoFisher Scientific, USA, reference #15596018) at -80°C for later analysis.

Experiment II variables: Mechanical stimulation and TGF- β 3 withdrawal

Experiment II was conducted under only HYP and simultaneously with Experiment I. Baseline tissues (from $n=4$ –6 donors) were randomly assigned into the TGF- β 3 withdrawal ($-T3$) or the TGF- β 3 continued ($+T3$) group where the growth factor was either removed or supplemented in the chondrogenic growth medium, respectively. Tissues in each group were further randomly assigned into two modalities of mechanical loading (dynamic compression, DC and cyclic hydrostatic pressure, CHP) or static

controls, all under HYP, resulting in six experimental groups: DC -T3, DC +T3, CHP -T3, CHP +T3, Static -T3, and Static +T3. Static control samples under HYP from the M23, M42, and M58 donors were used for both Experiments I and II analysis. Tissues in all groups were cultured with approximately 7.5 mL of medium per tissue construct (to equate the required volume of media for DC bioreactors), and media was changed once per week. Tissues were cultured for 3 weeks before harvest, and gene expression samples (2–3 technical replicates) from the mechanical loading groups were stored in TRIzol reagent 6 h after the last loading incident (to account for the time required to dismantle DC bioreactors) and kept at -80°C for later analysis.

Tissues in the DC experimental groups were cultured in commercial bioreactor chambers using a Biodynamic 5210 system (TA Instruments, USA) that permitted automated loading events. DC loading was applied four times a day from 20% to 30% strain at 1 Hz frequency for 10 min per loading incident followed by around 6 h of rest at 0% strain. Tissues in the CHP experimental groups were cultured in commercial bioreactors using a MechanoCulture TR (CellScale, ON, Canada). CHP loading was applied for 2 h, once per day, at 0.9 MPa hydrostatic pressure at 1 Hz frequency. When not loaded, tissues were cultured under static conditions (just like the static control groups) in non-attachment Petri-dishes with previously mentioned media volumes. Detailed loading protocols for DC and CHP are provided in Supplemental Figure S9.

Mechanical property assessment

A dynamic compression (DC) test identical to a single DC loading event was used to assess the mechanical properties of tissues (2–3 technical replicates) with the Biodynamic 5210 system (TA Instruments, USA). The cross-sectional area of the cylindrical tissues was first determined from gross morphology photos. For the test, tissues were placed between two platens and the initial height was determined by bringing the platens in contact with the tissue. The platens then ramped to 20% strain before a sine wave cyclic dynamic loading from 20% to 30% strain at 1 Hz frequency for 10 min. All tested tissues were able to reach equilibrium stress from cyclic loading within the given test period. Force was recorded as a function of time, and stress was calculated by normalizing the force to construct's cross-sectional area. Peak and equilibrium stress were calculated as the maximum recorded stress and the averaged stress from the relaxation curve, respectively, divided by the cross-sectional area. Peak and equilibrium moduli were then calculated as the respective stresses divided by the 10% dynamic strain increment. Detailed testing protocol is provided in Supplemental Figure S9. All tissues after mechanical testing were frozen at -80°C and used for subsequent biochemical assays, and the potential loss of GAG from compression should be systematically normalized across the study.

Histology, immunofluorescence, and biochemical analysis

The wet weight of tissues (4–5 technical replicates) intended for histology, biochemical, or mechanical property analyses was recorded after tissue harvest. Briefly, histology tissues (2 technical replicates, only one is presented) were fixed in 1 mL of 10% v/v buffered formalin (Fisher Scientific, MA, USA) overnight at 4°C , paraffin-embedded, and sectioned at $8\ \mu\text{m}$ thickness. Sections from approximately the middle region of the tissue were stained with Safranin-O, Fast Green FGF, and Hematoxylin (Sigma-Aldrich, USA, #MHS32-1L) or else labeled with primary antibodies against human types I, II, and X collagens (1:200 dilution of rabbit anti-human type I collagen, Cedarlane, Canada, #CL50111AP-1; 1:200 dilution of mouse anti-human type II collagen, Developmental Studies Hybridoma Bank, USA, #II-II6B3; 1:100 dilution of rabbit anti-human type X collagen, Abcam, UK, #ab58632) for immunofluorescent visualization by secondary antibodies (1:200 dilution of goat anti-rabbit, Abcam, UK, #ab150080; 1:200 dilution of goat anti-mouse, Abcam, UK, #ab150117) and DAPI (Cedarlane, Canada). Quantification of immunofluorescent images was conducted with a Python script.

For glycosaminoglycan (GAG) and DNA qualification, tissues that underwent mechanical property assessment (2–3 technical replicates) were digested first with hyaluronidase (Sigma-Aldrich, USA, #H6254) overnight at 37°C and then further digested with proteinase K (Sigma-Aldrich, USA, #P2308) at 56°C . GAG content was measured with the dimethyl methylene blue (DMMB, Sigma-Aldrich, USA, #341088) assay with a chondroitin sulfate standard (Sigma-Aldrich, USA, #C8529) and DNA content by the CyQUANT Cell Proliferation Assay (ThermoFisher Scientific, USA, #C7026).

RNA extraction, RT-qPCR, and next-generation RNA sequencing

Tissues for gene expression (2–3 technical replicates) were frozen at -80°C in TRIzol reagent (Life Technologies, USA) immediately upon harvest. RNA was isolated and extracted from ground tissue samples using the PuroSPIN Total DNA Purification Kit (Luna Nanotech, Canada) according to the manufacturer's protocols. RNA was reversely transcribed into cDNA with GoScript reverse transcriptase (Fisher Scientific, USA), and genes of interest were amplified by real-time quantitative polymerase chain reaction (RT-qPCR) using gene-specific primers listed in Supplemental Table S3. Gene expression was normalized to chosen housekeeping genes (*B-actin*, *RPL13A*, and *YWHAZ*) based on the coefficient of variation (CV) and M-value as measures of reference gene stability,⁸² and the data was presented using the $2^{-\Delta\Delta\text{CT}}$ method.^{83,84}

Next-generation RNA-sequencing ($n=3$ donors: M23, M42, M58) was performed on the Illumina NextSeq 500

platform with paired-end 42 bp × 42 bp reads, and FastQ files were obtained for further bioinformatics analysis. Supplemental Table S1 summarizes quality control metrics for the RNA-sequencing data. Briefly, the RNA Integrity Number (RIN) of all sequenced samples was acceptable, the average pre- and post-alignment read quality had Phred scores above 30, indicating high-quality reads, and the alignment algorithm resulted in an average of at least 98% alignment. The authenticity of the RNA-sequencing data was also validated against select RT-qPCR genes (Supplemental Figure S1), and the degree of correlation was determined with an R^2 value of 0.817, showing a strong correlation between the two transcription measurement methods.

Bioinformatics and statistical analysis

Next-generation sequencing data ($n=3$ donors: M23, M42, M58) were analyzed with the Partek® Flow® software (Version 10.0.21.0302, Copyright© 2021, Partek Inc, MO, USA). Briefly, raw input reads were first trimmed and then aligned to the reference human genome hg38 using the STAR 2.7.3a aligner. Aligned data were quantified to a transcript model (hg38-RefSeq Transcripts 99–2021–08–02) using the Partek E/M algorithm, and quantified reads were normalized in sequential order using the Add: 1.0, TMM, and Log 2.0 methods. Statistical analysis was performed separately for Experiments I and II using analysis of variance (ANOVA) for oxygen tension, TGF- β 3 presence, and mechanical stimulation with donors assigned as a random variable. Significant differentially expressed genes (DEGs) were determined by a combination of minimum total gene counts, adjusted p -values for false discovery rate (FDR) (q -values), and minimum absolute fold change (FC). Gene ontology enrichment, pathway enrichment, and visualization with Venn diagrams, heatmaps, PCA plots, and volcano plots were all conducted in Partek.

Statistical analyses were performed in Prism 9 (GraphPad) and the Partek® Flow® software. The statistical test used and p - or q -values are indicated in the respective figure legends. For most analyses, a one-way ANOVA with the Geisser-Greenhouse correction was used to compare each group with every other group, and a Tukey's multiple comparison test was used to find the adjusted p -value between each comparison. Statistical significance was determined with a threshold of 0.05.

Acknowledgements

We thank Tara Stach and the team at the Biomedical Research Centre from the University of British Columbia for their help with RNA sequencing.

Author contributions

All listed authors meet the Journal of Tissue Engineering criteria for authorship. DL, ZM, AS, and AA designed the study. DL, ZM, AS, XL, and AMS performed tissue culture. DL, ZM, and

MK performed RT-qPCR expression analysis. DL, ZM, and AA were responsible for RNA-seq data analysis with Partek Flow software. DL, ZM, and LW were responsible for mechanical testing and analysis. DL and ZM performed the statistical analysis and prepared tables and figures. DL, ZM, and AA wrote the manuscript with input from all co-authors. LW and AA were responsible for acquiring financial support and supervision of the study.

Declaration of Conflicting Interests

The author(s) declared no potential conflicts of interest with respect to the research, authorship, and/or publication of this article.

Funding

The author(s) disclosed receipt of the following financial support for the research, authorship, and/or publication of this article: DL: Natural Sciences and Engineering Research Council (NSERC Undergraduate Student Research Awards). ZM: Natural Sciences and Engineering Research Council (NSERC RQPIN-2018-06290 Adesida). AS: Alexander Graham Bell Scholarship Program (NSERC); Dean's Doctoral Award (Faculty of Medicine and Dentistry, University of Alberta); Queen Elizabeth II Scholarship program (Alberta government). XL: Natural Sciences and Engineering Research Council (NSERC). MK: Alberta Cancer Foundation-Mickleborough Interfacial Biosciences Research Program (ACF-MIBRP 27128 Adesida). AMS: Canadian Institutes of Health Research (CIHR MOP 125921 Adesida). LW: University of Alberta Pilot Seed Grant Program (UOFAB PSGP); University of Alberta Women and Children's Health Research Institute Innovation Grant (UOFAB WCHRIIG 3126). AA: Natural Sciences and Engineering Research Council (NSERC RGPIN-2018-06290 MOP 125921 Adesida); NSERC RTI-2019-00310 Adesida; the Canada Foundation for Innovation (CFI 33786); University Hospital of Alberta Foundation (UHF; RES0028185 Adesida); the Edmonton Orthopaedic Research Committee the Cliff Lede Family Charitable Foundation (RES00045921 Adesida); University of Alberta Pilot Seed Grant Program (UOFAB PSGP); University of Alberta Women and Children's Health Research Institute Innovation Grant (UOFAB WCHRIIG 3126); the Alberta Cancer Foundation-Mickleborough Interfacial Biosciences Research Program (ACF-MIBRP 27128 Adesida); University of Alberta Mid-Career Precision Health Innovator Award.




Data availability

The datasets presented in this study can be found in online repositories. The names of the repository/repositories and accession number(s) can be found below: GEO and GSE214720.

Ethical approval

Experimental methods and tissue procurement were conducted with approval from the University of Alberta's Health Research Ethics Board-Biomedical Panel (Study ID: Pro00018778).

ORCID iDs

David Xinzheyang Li  <https://orcid.org/0000-0002-1028-8445>
Alexander RA Szojka  <https://orcid.org/0000-0003-0334-9040>
Adetola B Adesida  <https://orcid.org/0000-0003-1798-6251>

Supplemental material

Supplemental material for this article is available online.

References

- Murray CJL, Vos T, Lozano R, et al. Disability-adjusted life years (DALYs) for 291 diseases and injuries in 21 regions, 1990–2010: a systematic analysis for the Global Burden of Disease Study 2010. *Lancet* 2012; 380: 2197–2223.
- Muthuri SG, McWilliams DF, Doherty M, et al. History of knee injuries and knee osteoarthritis: a meta-analysis of observational studies. *Osteoarthr Cartil* 2011; 19: 1286–1293.
- Peterson L, Minas T, Brittberg M, et al. Two- to 9-year outcome after autologous chondrocyte transplantation of the knee. *Clin Orthop Relat Res* 2000; 374: 212–234.
- Brittberg M, Lindahl A, Nilsson A, et al. Treatment of deep cartilage defects in the knee with autologous chondrocyte transplantation. *N Engl J Med* 1994; 331: 889–895.
- Marlovits S, Zeller P, Singer P, et al. Cartilage repair: generations of autologous chondrocyte transplantation. *Eur J Radiol* 2006; 57: 24–31.
- Benya PD and Shaffer JD. Dedifferentiated chondrocytes reexpress the differentiated collagen phenotype when cultured in agarose gels. *Cell* 1982; 30: 215–224.
- Benya PD, Padilla SR and Nimni ME. Independent regulation of collagen types by chondrocytes during the loss of differentiated function in culture. *Cell* 1978; 15: 1313–1321.
- Bornes TD, Adesida AB and Jomha NM. Mesenchymal stem cells in the treatment of traumatic articular cartilage defects: a comprehensive review. *Arthritis Res Ther* 2014; 16: 432.
- Mackay AM, Beck SC, Murphy JM, et al. Chondrogenic differentiation of cultured human mesenchymal stem cells from marrow. *Tissue Eng* 1998; 4: 415–428.
- Pittenger MF, Mackay AM, Beck SC, et al. Multilineage potential of adult human mesenchymal stem cells. *Science* 1999; 284: 143–147.
- Johnstone B, Hering TM, Caplan AI, et al. In Vitro Chondrogenesis of bone marrow-derived mesenchymal progenitor cells. *Exp Cell Res* 1998; 238: 265–272.
- Pelttari K, Winter A, Steck E, et al. Premature induction of hypertrophy during in vitro chondrogenesis of human mesenchymal stem cells correlates with calcification and vascular invasion after ectopic transplantation in SCID mice. *Arthritis Rheum* 2006; 54: 3254–3266.
- Mueller MB, Fischer M, Zellner J, et al. Hypertrophy in mesenchymal stem cell chondrogenesis: effect of TGF-beta isoforms and chondrogenic conditioning. *Cells Tissues Organs* 2010; 192: 158–166.
- Szójka ARA, Moore CN, Liang Y, et al. Engineered human meniscus' matrix-forming phenotype is unaffected by low strain dynamic compression under hypoxic conditions. *PLoS One* 2021; 16: e0248292.
- Zhang Z-Z, Chen Y-R, Wang S-J, et al. Orchestrated biomechanical, structural, and biochemical stimuli for engineering anisotropic meniscus. *Sci Transl Med* 2019; 11: eaao0750.
- Bahcecioglu G, Hasirci N, Bilgen B, et al. A 3D printed PCL/hydrogel construct with zone-specific biochemical composition mimicking that of the meniscus. *Biofabrication* 2019; 11: 025002.
- Meier EM, Wu B, Siddiqui A, et al. Mechanical stimulation increases knee meniscus gene RNA-level expression in adipose-derived stromal cells. *Plast Reconstr Surg Glob Open* 2016; 4: e864.
- Solorio LD, Vieregge EL, Dhimi CD, et al. Engineered cartilage via self-assembled hMSC sheets with incorporated biodegradable gelatin microspheres releasing transforming growth factor- β 1. *J Control Release* 2012; 158: 224–232.
- Ahearne M, Buckley CT and Kelly DJ. A growth factor delivery system for chondrogenic induction of infrapatellar fat pad-derived stem cells in fibrin hydrogels. *Biotechnol Appl Biochem* 2011; 58: 345–352.
- Diekman BO, Rowland CR, Lennon DP, et al. Chondrogenesis of adult stem cells from adipose tissue and bone marrow: induction by growth factors and cartilage-derived matrix. *Tissue Eng Part A* 2010; 16: 523–533.
- Wang Y, Kim U-J, Blasioli DJ, et al. In vitro cartilage tissue engineering with 3D porous aqueous-derived silk scaffolds and mesenchymal stem cells. *Biomaterials* 2005; 26: 7082–7094.
- Hennig T, Lorenz H, Thiel A, et al. Reduced chondrogenic potential of adipose tissue derived stromal cells correlates with an altered TGFbeta receptor and BMP profile and is overcome by BMP-6. *J Cell Physiol* 2007; 211: 682–691.
- Knudson CB. Hyaluronan and CD44: strategic players for cell-matrix interactions during chondrogenesis and matrix assembly. *Birth Defects Res C Embryo Today* 2003; 69: 174–196.
- Knudson W and Loeser RF. CD44 and integrin matrix receptors participate in cartilage homeostasis. *Cell Mol Life Sci* 2002; 59: 36–44.
- Wu S-C, Chang J-K, Wang C-K, et al. Enhancement of chondrogenesis of human adipose derived stem cells in a hyaluronan-enriched microenvironment. *Biomaterials* 2010; 31: 631–640.
- Wu S-C, Chen C-H, Chang J-K, et al. Hyaluronan initiates chondrogenesis mainly via CD44 in human adipose-derived stem cells. *J Appl Physiol* 2013; 114: 1610–1618.
- Khan WS, Adesida AB and Hardingham TE. Hypoxic conditions increase hypoxia-inducible transcription factor 2α and enhance chondrogenesis in stem cells from the infrapatellar fat pad of osteoarthritis patients. *Arthritis Res Ther* 2007; 9: R55.
- Adesida AB, Mulet-Sierra A and Jomha NM. Hypoxia mediated isolation and expansion enhances the chondrogenic capacity of bone marrow mesenchymal stromal cells. *Stem Cell Res Ther* 2012; 3: 9.
- Bader DL, Salter DM and Chowdhury TT. Biomechanical influence of cartilage homeostasis in health and disease. *Arthritis* 2011; 2011: 979032.
- Liu C, Abedian R, Meister R, et al. Influence of perfusion and compression on the proliferation and differentiation of bone mesenchymal stromal cells seeded on polyurethane scaffolds. *Biomaterials* 2012; 33: 1052–1064.
- Petri M, Ufer K, Toma I, et al. Effects of perfusion and cyclic compression on in vitro tissue engineered meniscus implants. *Knee Surg Sports Traumatol Arthrosc* 2012; 20: 223–231.
- Szójka ARA, Li DX, Sopcak MEJ, et al. Mechano-hypoxia conditioning of engineered human meniscus. *Front Bioeng Biotechnol* 2021; 9: 739438.

33. Szojka AR, Marqueti RC, Li DX, et al. Human engineered meniscus transcriptome after short-term combined hypoxia and dynamic compression. *J Tissue Eng* 2021; 12: 2041731421990842.
34. Lueckgen J, Kraemer E, Reiner T, et al. Altered susceptibility to mechanical loading by hypertrophic degeneration of chondrocytes. *Osteoarthr Cartil* 2021; 29: S211.
35. Bi W, Deng JM, Zhang Z, et al. Sox9 is required for cartilage formation. *Nat Genet* 1999; 22: 85–89.
36. Takahashi I, Nuckolls GH, Takahashi K, et al. Compressive force promotes sox9, type II collagen and aggrecan and inhibits IL-1beta expression resulting in chondrogenesis in mouse embryonic limb bud mesenchymal cells. *J Cell Sci* 1998; 111: 2067–2076.
37. Elder BD and Athanasiou KA. Hydrostatic pressure in articular cartilage tissue engineering: from chondrocytes to tissue regeneration. *Tissue Eng Part B Rev* 2009; 15: 43–53.
38. Mellor LF, Steward AJ, Nordberg RC, et al. Comparison of simulated microgravity and hydrostatic pressure for chondrogenesis of hASC. *Aerosp Med Hum Perform* 2017; 88: 377–384.
39. Zellner J, Mueller M, Xin Y, et al. Dynamic hydrostatic pressure enhances differentially the chondrogenesis of meniscal cells from the inner and outer zone. *J Biomech* 2015; 48: 1479–1484.
40. Gunja NJ, Uthamanthil RK and Athanasiou KA. Effects of TGF-beta1 and hydrostatic pressure on meniscus cell-seeded scaffolds. *Biomaterials* 2009; 30: 565–573.
41. Carroll SF, Buckley CT and Kelly DJ. Cyclic hydrostatic pressure promotes a stable cartilage phenotype and enhances the functional development of cartilaginous grafts engineered using multipotent stromal cells isolated from bone marrow and infrapatellar fat pad. *J Biomech* 2014; 47: 2115–2121.
42. Miyanishi K, Trindade MC, Lindsey DP, et al. Dose- and time-dependent effects of cyclic hydrostatic pressure on transforming growth factor-beta3-induced chondrogenesis by adult human mesenchymal stem cells in vitro. *Tissue Eng* 2006; 12: 2253–2262.
43. Miyanishi K, Trindade MCD, Lindsey DP, et al. Effects of hydrostatic pressure and transforming growth factor-β 3 on adult human mesenchymal stem cell chondrogenesis in vitro. *Tissue Eng* 2006; 12: 1419–1428.
44. Wagner DR, Lindsey DP, Li KW, et al. Hydrostatic pressure enhances chondrogenic differentiation of human bone marrow stromal cells in osteochondrogenic medium. *Ann Biomed Eng* 2008; 36: 813–820.
45. Finger AR, Sargent CY, Dulaney KO, et al. Differential effects on messenger ribonucleic acid expression by bone marrow-derived human mesenchymal stem cells seeded in agarose constructs due to ramped and steady applications of cyclic hydrostatic pressure. *Tissue Eng* 2007; 13: 1151–1158.
46. Li Y, Zhou J, Yang X, et al. Intermittent hydrostatic pressure maintains and enhances the chondrogenic differentiation of cartilage progenitor cells cultivated in alginate beads. *Dev Growth Differ* 2016; 58: 180–193.
47. Leys L, Bouwmeester T, Kim SH, et al. Frzb-1 is a secreted antagonist of Wnt signaling expressed in the Spemann organizer. *Cell* 1997; 88: 747–756.
48. Hendig D, Zarbock R, Szliska C, et al. The local calcification inhibitor matrix Gla protein in pseudoxanthoma elasticum. *Clin Biochem* 2008; 41: 407–412.
49. Narayanan K, Ramachandran A, Hao J, et al. Dual functional roles of dentin matrix protein 1. Implications in biomineralization and gene transcription by activation of intracellular Ca²⁺ store. *J Biol Chem* 2003; 278: 17500–17508.
50. Drabek K, van de Peppel J, Eijken M, et al. GPM6B regulates osteoblast function and induction of mineralization by controlling cytoskeleton and matrix vesicle release. *J Bone Miner Res* 2011; 26: 2045–2051.
51. Asch AS, Silbiger S, Heimer E, et al. Thrombospondin sequence motif (CSVTCG) is responsible for CD36 binding. *Biochem Biophys Res Commun* 1992; 182: 1208–1217.
52. Cecil DL, Appleton CT, Polewski MD, et al. The pattern recognition receptor CD36 is a chondrocyte hypertrophy marker associated with suppression of catabolic responses and promotion of repair responses to inflammatory stimuli. *J Immunol* 2009; 182: 5024–5031.
53. Pfander D, Cramer T, Deuerling D, et al. Expression of thrombospondin-1 and its receptor CD36 in human osteoarthritic cartilage. *Ann Rheum Dis* 2000; 59: 448–454.
54. Zupan J, Mencej-Bedrac S, Jurković-Mlakar S, et al. Gene-gene interactions in RANK/RANKL/OPG system influence bone mineral density in postmenopausal women. *J Steroid Biochem Mol Biol* 2010; 118: 102–106.
55. Heinonen J, Taipaleenmäki H, Roering P, et al. Snorc is a novel cartilage specific small membrane proteoglycan expressed in differentiating and articular chondrocytes. *Osteoarthr Cartil* 2011; 19: 1026–1035.
56. Gruber BL, Mienaltowski MJ, MacLeod JN, et al. Tenascin-C expression controls the maturation of articular cartilage in mice. *BMC Res Notes* 2020; 13: 78.
57. Schwaerzer GK, Hiepen C, Schrewe H, et al. New insights into the molecular mechanism of multiple synostoses syndrome (SYNS): mutation within the GDF5 knuckle epitope causes noggin-resistance. *J Bone Miner Res* 2012; 27: 429–442.
58. Schlegel W, Albrecht C, Eckl P, et al. Dedifferentiation of human articular chondrocytes is associated with alterations in expression patterns of GDF-5 and its receptors. *J Cell Mol Med* 2009; 13: 3398–3404.
59. Feng Q, Li S, Ma HM, et al. LGR6 activates the Wnt/β-catenin signaling pathway and forms a β-catenin/TCF7L2/LGR6 feedback loop in LGR6high cervical cancer stem cells. *Oncogene* 2021; 40: 6103–6114.
60. Choi Y-A, Lim J, Kim KM, et al. Secretome analysis of human BMSCs and identification of SMOC1 as an important ECM protein in osteoblast differentiation. *J Proteome Res* 2010; 9: 2946–2956.
61. Williams JA, Kondo N, Okabe T, et al. Retinoic acid receptors are required for skeletal growth, matrix homeostasis and growth plate function in postnatal mouse. *Dev Biol* 2009; 328: 315–327.
62. Otsuka F, Hino J, Matsumoto Y, et al. BMP-3b inhibits osteoblast differentiation via Smad2/3 pathway by counteracting Smad1/5/8 signaling. In: *Endocrine Abstracts*. Bioscientifica, 2012.
63. Massagué J. TGF-beta signal transduction. *Annu Rev Biochem* 1998; 67: 753–791.

64. Tuli R, Tuli S, Nandi S, et al. Transforming growth factor-beta-mediated chondrogenesis of human mesenchymal progenitor cells involves N-cadherin and mitogen-activated protein kinase and Wnt signaling cross-talk. *J Biol Chem* 2003; 278: 41227–41236.
65. Erickson IE, Huang AH, Chung C, et al. Differential maturation and structure-function relationships in mesenchymal stem cell- and chondrocyte-seeded hydrogels. *Tissue Eng Part A* 2009; 15: 1041–1052.
66. Patil AS, Sable RB and Kothari RM. An update on transforming growth factor- β (TGF- β): sources, types, functions and clinical applicability for cartilage/bone healing. *J Cell Physiol* 2011; 226: 3094–3103.
67. Wang W, Rigueur D and Lyons KM. TGF β signaling in cartilage development and maintenance. *Birth Defects Res C Embryo Today* 2014; 102: 37–51.
68. Park JS, Shim M-S, Shim SH, et al. Chondrogenic potential of stem cells derived from amniotic fluid, adipose tissue, or bone marrow encapsulated in fibrin gels containing TGF- β 3. *Biomaterials* 2011; 32: 8139–8149.
69. Bian L, Zhai DY, Tous E, et al. Enhanced MSC chondrogenesis following delivery of TGF- β 3 from alginate microspheres within hyaluronic acid hydrogels in vitro and in vivo. *Biomaterials* 2011; 32: 6425–6434.
70. Tang QO, Shakib K, Heliotis M, et al. TGF-beta3: A potential biological therapy for enhancing chondrogenesis. *Expert Opin Biol Ther* 2009; 9: 689–701.
71. Pfeifer CG, Karl A, Kerschbaum M, et al. TGF- β signalling is suppressed under Pro-Hypertrophic conditions in MSC chondrogenesis due to TGF- β receptor downregulation. *Int J Stem Cells* 2019; 12: 139–150.
72. Clark CR and Ogden JA. Prenatal and postnatal development of human knee joint menisci. *Iowa Orthop J* 1981; 1: 20–27.
73. McNicol D and Roughley PJ. Extraction and characterization of proteoglycan from human meniscus. *Biochem J* 1980; 185: 705–713.
74. Barry F, Boynton RE, Liu B, et al. Chondrogenic differentiation of mesenchymal stem cells from bone marrow: differentiation-dependent gene expression of matrix components. *Exp Cell Res* 2001; 268: 189–200.
75. Kim J, Boys AJ, Estroff LA, et al. Combining TGF- β 1 and mechanical anchoring to enhance collagen fiber formation and alignment in tissue-engineered menisci. *ACS Biomater Sci Eng* 2021; 7: 1608–1620.
76. Chen S and Birk DE. The regulatory roles of small leucine-rich proteoglycans in extracellular matrix assembly. *FEBS J* 2013; 280: 2120–2137.
77. Byers BA, Mauck RL, Chiang IE, et al. Transient exposure to transforming growth factor beta 3 under serum-free conditions enhances the biomechanical and biochemical maturation of tissue-engineered cartilage. *Tissue Eng Part A* 2008; 14: 1821–1834.
78. Remya NS and Nair PD. Mechanoresponsiveness of human umbilical cord mesenchymal stem cells in *in vitro* chondrogenesis-A comparative study with growth factor induction. *J Biomed Mater Res A* 2016; 104: 2554–2566.
79. Elkhenany HA, Szojka ARA, Mulet-Sierra A, et al. Bone marrow mesenchymal stem cell-derived tissues are mechanically superior to meniscus cells. *Tissue Eng Part A* 2021; 27: 914–928.
80. Liang Y, Idrees E, Andrews SHJ, et al. Plasticity of human meniscus fibrochondrocytes: A study on effects of mitotic divisions and oxygen tension. *Sci Rep* 2017; 7: 12148.
81. Ma Z, Li DX, Kunze M, et al. Engineered human meniscus in modeling Sex differences of knee osteoarthritis in vitro. *Front Bioeng Biotechnol* 2022; 10: 823679.
82. Hellemans J, Mortier G, De Paepe A, et al. QBase relative quantification framework and software for management and automated analysis of real-time quantitative PCR data. *Genome Biol* 2007; 8: R19.
83. Schmittgen TD and Livak KJ. Analyzing real-time PCR data by the comparative CT method. *Nat Protoc* 2008; 3: 1101–1108.
84. Livak KJ and Schmittgen TD. Analysis of relative gene expression data using real-time quantitative PCR and the 2- $\Delta\Delta$ CT method. *Methods* 2001; 25: 402–408.